International Journal of Disaster Risk Reduction 116 (2025) 105005

Contents lists available at ScienceDirect

International Journal of Disaster Risk Reduction

journal homepage: www.elsevier.com/locate/ijdrr

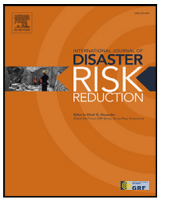

Bridging IAA and IDA: A Conceptual framework, application, and implication in risk assessment

M. Amin Hariri-Ardebili [a,b,*], Giacomo Sevieri [c], Carlo Resta [d], Anna De Falco [d], Sissy Nikolaou [b], Siamak Sattar [b]

[a] University of Maryland, College Park, MD, USA
[b] National Institute of Standards and Technology, Gaithersburg, MD, USA
[c] Aon Reinsurance, Lucca, Tuscany, Italy
[d] University of Pisa, Largo Lucio Lazzarino 1, Pisa, Italy

ARTICLE INFO

Keywords:
Artificial acceleration
IDA
Wave deconvolution
Seismic response
Soil/rock-structure interaction

ABSTRACT

Quantifying the progressive failure of infrastructures under seismic excitation is crucial for accurate risk evaluation. Such analyses often necessitate detailed structural evaluations using numerous ground motion records across a range of seismic intensities. This study proposes intensifying artificial acceleration (IAA) as a novel method for approximating the seismic response of structural systems. The performance of IAA is evaluated in comparison with traditional single-record incremental dynamic analysis (IDA), employing a benchmark geo-structure problem that incorporates soil/rock-structure interaction. This research assesses the efficacy and precision of IAA for nonlinear systems with and without wave propagation in the foundation. Wave deconvolution is applied to both IAA and IDA, and a damage index is calculated to quantify crack extension. Serving as a proof of concept, the results highlight a promising alignment between IAA and IDA outcomes, with IAA offering significant reductions in computational demand. The paper concludes with a conceptual framework for integrating ground motion-compatible IAAs into streamlined risk assessment processes.

1. Introduction

Seismic assessment of infrastructures is an essential step to estimate the risk and evaluate the safety of communities [1]. It can be broadly categorized into the following methods: (1) seismic coefficient method [2], (2) equivalent lateral force method, (3) response spectrum modal analysis method, (4) time history modal analysis method, and (5) time history-time integration (THTI) procedure. In the latter, the equations of motion are integrated directly in the time domain, and it can be used for both linear and nonlinear finite element models.

While the THTI procedure[1] provides a complete picture of a structure's response when subjected to a known seismic input, it does not account for uncertainties on loads. Moreover, it only provides the response at a particular seismic intensity level (SIL). To overcome these challenges, the adoption of probabilistic methods seems unavoidable. Some of the existing and widely

* Corresponding author at: National Institute of Standards and Technology, Gaithersburg, MD, USA.
E-mail address: amin.hariri@nist.gov (M.A. Hariri-Ardebili).

[1] The THTI procedure referenced in this paper corresponds to the numerical integration of the equations of motion for a dynamic system under a single deterministic input. This approach typically solves the governing equations $\mathbf{M}\ddot{\mathbf{u}}(t)+\mathbf{C}\dot{\mathbf{u}}(t)+\mathbf{K}\mathbf{u}(t)=\mathbf{F}(t)$, where $\mathbf{M}$, $\mathbf{C}$, and $\mathbf{K}$ are the mass, damping, and stiffness matrices, respectively; $\mathbf{u}(t)$, $\dot{\mathbf{u}}(t)$, and $\ddot{\mathbf{u}}(t)$ are the displacement, velocity, and acceleration response vectors; and $\mathbf{F}(t)$ is the external force vector, here representing a specific ground motion.

https://doi.org/10.1016/j.ijdrr.2024.105005
Received 29 April 2024; Received in revised form 20 November 2024; Accepted 22 November 2024
Available online 19 December 2024

used probabilistic methods include: incremental dynamic analysis (IDA) [3], cloud analysis (CLA) [4], and multiple-stripe analysis (MSA) [5].

The (multi-record) IDA method considers multiple ground motion records at various SILs and thus it eliminates the dependence of results on the characteristics of the seismic input. In the IDA method, a suite of ground motion records should be compiled and scaling levels should be selected for each record. The IDA curve can be generated for any set of structural responses. In turn, these responses are interpolated for each record and all records are summarized by appropriate statistical approaches. It is evident that conducting nonlinear analyses of complex structures, such as bridges and dams, by using a large number of records at various SILs (and, finally, extracting and summarizing the results) is very time-consuming, and practically impossible for practitioners.

The quest to develop new analysis methods that can eliminate the shortcomings of aforementioned methods led to the development of the endurance time analysis (ETA) technique [6]. ETA is a time history-based dynamic pushover procedure, which uses a special intensifying artificial acceleration (IAA) as an input to analyze the structural system. An IAA evaluates the structural behavior from the linear elastic to the nonlinear range and, finally, to collapse level, within a single simulation. The major difference between ETA and IDA methods is that the former uses a limited number of inputs (typically one to three) to evaluate the dynamic behavior of the structure at various SILs, while the IDA requires hundreds of nonlinear simulations. However, IDA estimates the ground motion record-to-record (RTR) variability, while ETA does not have this capability [7]. The fundamentals of the ETA method can be found in Estekanchi and Vafai [8] with a state-of-the-knowledge review in Estekanchi et al. [9].

The key parameter in the successful implementation of the ETA method lies in generating a reliable IAA [10]. All previous studies on the ETA method are based on a generic set of IAAs, which are optimized based on smoothed (or codified) response spectra. For most validation purposes [11], the process involves determining the extent to which a conceptual model accurately represents real-world physical phenomena for the intended use. Through validation, evidence is provided that the chosen conceptual model is correct. In this paper, we consider the proposed IAA as said "conceptual method" and evaluate its accuracy by comparing it to IDA, which is considered to be the real-world application consisting in incrementally scaling ground motion records and performing dynamic analysis. It should be stressed that this assumption does not imply that IDA is the definitive or true method for evaluating seismic response of structures. In fact, several studies have highlighted issues related to using very large scale factors for ground motions. However, for the purposes of this study, the IAA was generated using a single ground motion record, and hence a single-record IDA is used as a reference method for validation. Moreover, a validation process involves estimation of errors, addressing the comfort level, assessing accuracy and credibility. However, the structure's response must be subjected to a particular ground motion record. Thus, the main contribution of this paper is to compare the dynamic response of a coupled geo-structural system using single-record IDA and IAA methods. This procedure is schematically illustrated in Fig. 1. First, an IAA is generated which is compatible with the target ground motion record (the criteria for such compatibility are discussed later). Second, the ground motion-compatible IAA is applied to the computational platform (e.g., finite element model), and a continuous response of the system is recorded (i.e., IAA curve). Third, the ground motion record itself is scaled to N different SILs, and a total of N nonlinear simulations are performed. The discrete results of these N simulations are interpolated to form a reference IDA curve [3]. Finally, the IAA and IDA curves are compared and their (potential) discrepancies are evaluated for various modeling strategies. In this paper, the nonlinear models for the geo-structure are considered. Next to this, the foundation is modeled with and without wave propagation assumptions. If the results show inconsistency between IDA and IAA, the process of IAA generation needs to be improved. If not, one can use the IAA as an alternative to single-record IDA, in order to reduce the computational effort. For verification purposes, only the ground motion's horizontal component is considered in this paper, and the impact of multi-component ground motion will be studied in the future.

An important field of application of a successful IAA is risk assessment. The analysis of risk, and catastrophe models more specifically, require the derivation of vulnerability curves. The process hinges on the evaluation of structural fragility under different damage scenarios and limit states, which entails a high computational burden and may therefore benefit from advancements on the topic. This work represents a first step towards the reduction of said burden without any significant loss of accuracy. The latter aspect is of central importance when dealing with structures such as dams, where simplified approaches may produce unsatisfying results, mainly due to the necessity of taking into account the mutual interactions between soil, structure and basin, and because of a general difficulty in standardizing the failure modes of dams.

The novelties and contribution of the authors can be summarized as follows: (1) validation of the IAA with respect to the single-record IDA method, (2) generation and validation of ground motion compatible IAA, (3) deconvolution of IAA records and comparing the results with respect to real ground motions, and (4) comparison of the IAA for soil/rock-structure interaction problems with massed and massless foundation models.

The remaining sections of this paper focus on the following topics: Section 2 discusses the theory and concept of the ground motion compatible IAA records; Section 3 presents a benchmark case study, its finite element model, and a description of the solution algorithm; Section 4 compares the selected target ground motion record and the corresponding IAA, and Section 5 validates the proposed method and presents the comparison results.

2. Theory of ground motion-compatible IAA

As mentioned earlier, the ETA is a dynamic pushover procedure used to estimate the seismic performance of the structures when subjected to a pre-designed excitation function called IAA. These simulated acceleration functions shake the structure from a low SIL, with a structural response in the elastic range, progressing to a high SIL that induces inelastic behavior, and finally leading to failure. The structure experiences the full spectrum of response variation during a single dynamic analysis. The structural performance is

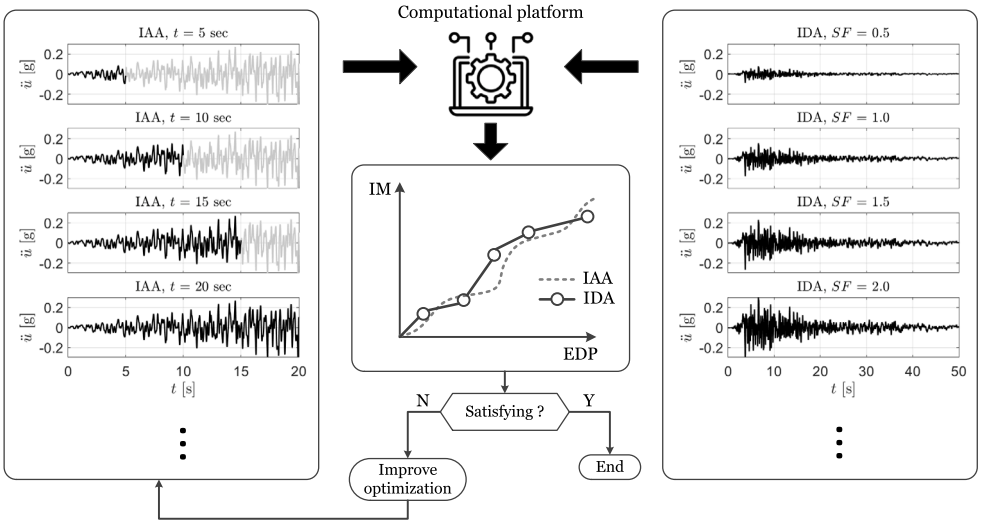

Fig. 1. A conceptual framework for validating IAA with respect to single-record IDA results.

assessed based on the duration of time the structure can sustain (or rather endure) the imposed artificial excitation. Typically a longer endurance time (before failure) is an indication of a stronger (i.e., well-designed) structure.

The IAA is an artificially-designed intensifying acceleration time series, where the response spectra of the IAA linearly increase with time. Ideally (and not necessarily), the profile of the acceleration time history and response spectrum increases linearly with time. Multiple studies investigated the generation and application of such intensifying acceleration time series. The pioneering work belongs to Nozari and Estekanchi [10] that generated IAAs compatible with a smoothed acceleration and displacement response spectra. Mashayekhi et al. [12] introduced the hysteretic energy concept, as well as cumulative absolute velocity [13] in IAA generation. Pang et al. [14] modified the IAAs by adding the corrected tapered cosine wavelets in the specific time domain to match the corresponding target spectra. Li et al. [15] improved the IAAs by adding more restriction to their target time and presenting it as a function of both peak ground acceleration (PGA) and Arias intensity. Zhang et al. [16] proposed a modification for the IAA by using a time-domain spectral matching method.

In this paper, the IAA is generated in a way that induces a seismic demand that is compatible with an actual ground motion record. Usually, code spectrum or average spectra of a ground motion record set (e.g., FEMA P695) are used as the target spectrum to produce the IAAs. However, this paper proposes, for the first time, the idea of generating IAAs that are compatible with a particular ground motion record. Acceleration spectra, nonlinear displacement, and absorbed hysteretic energy are included in the IAA generating process. Unconstrained nonlinear optimization is used to simulate IAAs where the objective function is to compute the differences between dynamic characteristics of the IAAs and their intended target values. In this paper, the following objective function is used [12]:

$$F_{IAA}(\ddot{u}_g) = \int_{T=0}^{T_{max}} \int_{t=0}^{t_{max}} \left[S_a(t,T) - S_a^*(t,T)\right]^2 \, \mathrm{d}t \, \mathrm{d}T + \int_{\mu=1}^{\mu_{max}} \int_{T=0}^{T_{max}} \int_{t=0}^{t_{max}} \left\{ \begin{array}{c} \alpha_{u_m} \left[u_m(t,T,\mu) - u_m^*(t,T,\mu)\right]^2 \\ +\alpha_{E_H} \left[E_H(t,T,\mu) - E_H^*(t,T,\mu)\right]^2 \end{array} \right\} \mathrm{d}t \, \mathrm{d}T \, \mathrm{d}\mu \quad (1)$$

where $\ddot{u}_g(t)$ is the acceleration time series of the IAA, and $S_a(t,T)$, $u_m(t,T,\mu)$, and $E_H(t,T,\mu)$ are the acceleration spectra, the nonlinear displacement, and the hysteretic energy (by integration of hysteresis loop area) of the IAA, whereas $S_a^*(t,T)$, $u_m^*(t,T,\mu)$ and $E_H^*(t,T,\mu)$ are the target acceleration spectra, the nonlinear displacement, and the hysteretic energy of a particular ground motion at time t, period T, and ductility ratio μ. In this equation, α refers to optimization coefficient. The weight factor α_{u_m} is computed by taking the double integral of the squared target spectral acceleration $S_a^*(t,T)$ over the desired period and time intervals and dividing it by the double integral of the squared target nonlinear displacement $u_m^*(t,T,\mu)$ over the same intervals. The weight factor α_{E_H} is computed in a similar way but using target hysteretic energy $E_H^*(t,T,\mu)$ instead of nonlinear displacement.

Dynamic characteristics of the IAA are extracted through nonlinear and linear responses of single degree of freedom systems (SDOF). These SDOFs are characterized by their periods and strength levels. The strength level or capacity is denoted by $F_y(T,\mu)$ and is a function of period and ductility ratio. $F_y(T,\mu)$ is the minimum lateral strength capacity that an SDOF system with a period of T requires to avoid the average ductility ratio demands larger than μ under a particular ground motion record. To evaluate the objective function, t is discretized at 2^{11} = 2048 points[2] with a time increment 0.01 s; T is discretized at 120 points, which are logarithmically distributed between 0.02 and 5.00 s; and μ is discretized at three points: 2, 4, and 8.

[2] The total number of discretized points in IAA is not critically important. The IAA continues to run until failure is reached, so any factor of 2^n can be used for their generation. For example, they can be generated to have 1024 points (10.24 s), 2048 points (20.48 s), 4096 points (40.96 s), or any other number. If

A linear profile is used in this study; therefore, $S_a^*(t,T)$ is calculated as follow:

$$S_a^*(t,T) = \frac{t}{t_{\text{trg}}} S_a^{\text{GM}}(T) \tag{2}$$

where $S_a^{\text{GM}}(T)$ represents the target acceleration spectra, which is the acceleration spectra of a particular ground motion. t_{trg} is the time at which the IAA should match the target spectrum. Although t_{trg} is optional, it is fixed to be 10 s in this paper. This means that the response spectrum from the generated IAA should match reasonably the target one at $t = 10$ s. For very long-duration ground motions, such as those recorded in subduction zones, a larger target time may be more appropriate.

On the other hand, $u_m^*(t,T,\mu)$ and $E_H^*(t,T,\mu)$ are calculated as follows:

$$u_m^*(t,T,\mu) = h_u(t,T,\mu) \times u_m^{\text{GM}}(T,\mu) \tag{3}$$

$$E_h^*(t,T,\mu) = h_{E_h}(t,T,\mu) \times E_H^{\text{GM}}(T,\mu) \tag{4}$$

where $u_m^{\text{GM}}(T,\mu)$ and $E_H^{\text{GM}}(T,\mu)$ are the nonlinear displacement and hysteretic energy imposed by a particular ground motion record. $h_u(t,T,\mu)$ and $h_{E_h}(t,T,\mu)$ are variation functions of target nonlinear displacement and hysteretic energy in time that are calculated for that particular ground motion [12]. $h_u(t,T,\mu)$ is computed by scaling the ground motion multiple times and calculating the demands for each scale factor, λ. The scale factor λ can be transformed to time, t, using the transformation function $\lambda = t/t_{\text{trg}}$. $h_{E_h}(t,T,\mu)$ represents the time-dependent variations of the target hysteretic energy demand as a function of a specific period and ductility values.

It is noteworthy that while the duration of the target ground motion record is not explicitly considered as a variable for IAA optimization (Eq. (1)), the significance of acceleration pulse duration is recognized and indirectly addressed during the IAA optimization through the inclusion of hysteretic energy compatibility. This approach ensures that the dynamic response reflects a balance between acceleration intensity and duration within the model's framework. Further discussion about the consistency of strong-motion duration in IAAs and real ground motion records can be found in [17].

In this paper, the IAA is generated for a single ground motion record, assuming the mainshock is the dominant event. However, in reality, the mainshock is typically followed by one or more aftershocks [18], some of which may be strong enough to cause further damage to the structure. This was indeed reported during the 2023 Türkiye earthquake sequence as reported by Hariri-Ardebili and Tosun [19]. The proposed IAA method can be applied to such cases by developing different intensifying acceleration functions for the mainshock and each aftershock. For deterministic simulations, both mainshock IAA and aftershock IAAs should be applied until a cut-off time associated with the target response spectra. This is determined by comparing the response spectra using Eq. (2). For probabilistic simulations (i.e., IDA-type analysis as discussed in this paper), multiple portions of the mainshock IAA (for example, 0–2 s, 0–4 s, etc.) should be separately combined with the entire aftershock IAA. Since this topic extends beyond the scope of this paper, interested readers are referred to Farivarrad and Estekanchi [20] for a comprehensive discussion on the modeling of multiple earthquakes with IAA method.

3. Case study problem: History and modeling

In this paper, a benchmark geo-structure problem (i.e., Pine Flat Dam) is adopted. The United States Society of Dams (USSD) and the International Committee on Large Dams (ICOLD) have organized two benchmark workshops in 2018 and 2019 in which the seismic response of this dam is asked to be predicted under a (generic) IAA. The summary of those two workshops can be found in [21,22]. This dam was also extensively studied during the 1970s and 1980s at the University of California at Berkeley [23–26].

There are also other reasons to use Pine Flat Dam as a case study. First, the finite element model of this dam includes foundation–structure interaction which is suitable to study the wave propagation (one of the objectives of this paper). Such an advantage is rarely found in framed structures, for which the soil/rock-structure interaction is typically ignored. Second, the application of the IAA for seismic analysis of complex infrastructures is more cost-effective compared to simple framed structures. While the nonlinear analysis of a framed structure may take only a few minutes, the seismic analysis of a dam takes several hours or a day. Therefore, we put the priority in this paper to analyze a dam as a case study. Yet, a similar method can be applied to other engineering structures (e.g., steel and concrete buildings, bridges, pipes, piles, etc.).

The IAA has been used to analyze a variety of engineering structures; however, those related to the analysis of geo-structure including the soil/rock-structure interaction are seismic response analysis of an arch dam subjected to IAA at different SILs including the linear behavior [27] and nonlinear damage response [28]. Hariri-Ardebili and Saouma [29] combined IAA with the concept of damage index (DI) to quantify the progressive damage. Proceedings of the ICOLD published over ten papers on the seismic analysis of the structure using IAA [30]. Liang et al. [31] and Xu et al. [32] conducted a correlation study between seismic intensity measures and nonlinear response of a dam-foundation system via generic IAAs. Xu et al. [33] used the IAAs to evaluate the seismic damage response of a dam-foundation system and compared the results with the IDA method.

In this paper, the benchmark problem introduced by ICOLD [22,34] is adopted. A two-dimensional finite element model of the central non-overflow section is prepared using ABAQUS 6.14 [35]. The finite element model consists of a 121.9-m-high dam with

the IAA duration is too short, there is a risk that failure is not reached before the IAA ends. If the IAA duration is too long, such as 40.96 s, there is a waste of resources in the optimization of IAA because failure may occur well before the total duration. For most engineering structures, 20.48 s is optimal.

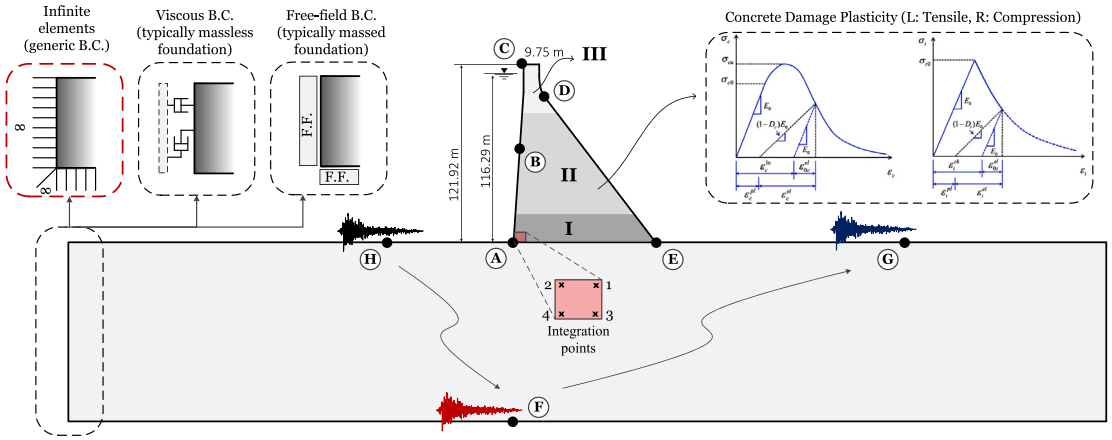

Fig. 2. Finite element model of dam-reservoir-foundation system, including foundation boundary conditions, and wave propagation.

a maximum width at the base of 95.8 m, and a 700-m-long, 122-m-deep foundation block together with a 310-m-long, 116-m-deep reservoir. The foundation is modeled as a linear elastic domain composed of 4520 four-node plane stress elements, while the dam body includes 1391 elements (typical element size is 2 m-by-2 m with 50 elements at the dam-foundation interface). The concrete damage plasticity model [36] is used for the dam body. The reservoir is modeled with 4012 four-node bi-linear acoustic elements considering compressible fluid[3] The pressure in the fluid elements only accounts for the hydrodynamic effects, and an equivalent hydrostatic pressure needs to be directly applied at the fluid–solid (i.e., dam or foundation) interfaces. A zero-pressure condition is imposed at the upper surface of the acoustic domain, while low-reflecting boundary conditions [37], modeling the unboundedness of the reservoir, are applied at the far-end boundary of the reservoir. Dynamic analyses are carried out using an implicit direct time-integration approach. An automatic time step incrementation scheme, based on half-step residual control, are used to optimize the balance between computational efficiency and solution accuracy. This adaptive scheme adjusts the time step size (a value between 1e−2 to 1e−7 s) in response to the equilibrium residual error measured halfway through each time increment. A 5e−3 is used for error on residuals in balance equations for displacement field. Moreover, the largest correction to nodal variables by each Newton iteration is set to 1e−2 times the largest change in nodal variable in the increment. Fig. 2 illustrates the finite element model including the key point in which the responses will be extracted and discussed.

To investigate the IAA wave propagation, two types of the foundation model assumptions are considered: the massless model, and massed model. While the former model is commonly used among practitioners, the latter is broadly recognized as more reliable in the scientific community [37,38]. This additional assumption is then beneficial for the research herein, even though it adds another level of complexity in the comparison itself, as the two foundation models significantly affect the soil/rock-structure interaction. The soil/rock-structure interaction is commonly seen as comprising two main contributions: the kinematic interaction, and the inertial interaction [39]. The former is governed by the rock flexibility, while the latter is generated by the elastic waves that develop under the dynamic loads. The inertial interaction promotes energy transport through the rock volume. Such a phenomenon, that carries energy away from the structure, is often referred to as "radiation damping". In seismic analysis with the massless model, the inertial interaction is completely disregarded. The wave velocity in the foundation becomes infinite, and the seismic input, applied at the boundaries of the domain, reaches instantaneously to the base of the structure which takes all kinetic energy [40].

These two different modeling assumptions affect the outcome of dynamic analysis [37]. Therefore, it is vital to choose proper boundary conditions and also pre-process the seismic input to make these two assumptions comparable. In this paper, ABAQUS built-in infinite elements are used to model the unboundedness of the rock domain. The dynamic implementation of the infinite elements (based on Lysmer and Kuhlemeyer [41]) has a similar formulation to traditional finite elements, except for the infinite extent of the element region and shape function in one direction.

In addition to the unboundedness of the rock domain, the massed model needs further elaboration on the seismic input. The inertial component of the soil/rock-structure interaction leads to higher damping, which reduces the seismic input and a massed rock acts as a filter for the seismic input. In other words, assuming that both the massless and massed foundation models experience the same dynamic excitation applied at the bottom of the foundation domain, i.e., point F in Fig. 2, the recorded acceleration at the free surface, i.e., point G, is different for them. The seismic input of the massed foundation model has then to be deconvolved to have an acceleration in point G which is similar to the massless model. Further discussion on the deconvolution process is provided later in this section.

[3] Compressible fluid elements account for changes in fluid density due to pressure variations. They incorporate the bulk modulus (compressibility) to model the pressure-volume relationship. Compressible fluid elements support the propagation of pressure (acoustic) waves with finite speed. These elements often use specific equations of state to define the relationship between pressure, volume, and temperature.

Table 1
Elastic properties of concrete and rock foundation.

ρ_c [kg/m^3]	E_c [MPa]	υ_c	$\beta_{K,c}$ [s]	ρ_r [kg/m^3]	E_r [MPa]	υ_r	$\beta_{K,r}$ [s]
2483	22,410	0.2	0.0022	2483	22,410	0.2	0.0044

Table 2
Concrete damage plasticity model parameters.

Ψ [°]	ε [–]	σ_{b0}/σ_{c0} [–]	Λ [–]	f_t [MPa]	f_c [MPa]	G_f [N/m]
36.31	0.1	1.16	0.66	2	20	250

The Rayleigh damping equates to approximately 2% for the frequency in a range of 1.5 and 2.8 Hz, assuming a damping matrix **C** composed of the stiffness proportional part only. The stiffness coefficient β_K is larger than zero, while the mass coefficient α_M is equal to zero. Løkke and Chopra [38] provides a discussion on the application of Rayleigh damping to simulate the dam-foundation systems and the usefulness of the only stiffness proportional part of the damping matrix. When cracks extend through the concrete continuum, the mass proportional part of the damping matrix generates spurious damping forces that prohibit sliding and overturning of the sections above an open crack. On the other hand, the element damping forces due to the stiffness proportional part of the damping matrix are proportional to deformation rates in the element, making its application more appealing for these structural problems. With this assumption, **C** is constructed by assembling the stiffness proportional damping sub-matrices of dam and foundation, $\mathbf{C}_{concrete}$ and $\mathbf{C}_{rock}$, respectively. The dam and foundation stiffness coefficients, $\beta_{K,c}$ and $\beta_{K,r}$, are finally calibrated through an optimization process in the frequency domain, targeting a 2% damping in the frequency range reported above. Table 1 lists the damping stiffness coefficients together with the elastic properties of the concrete and rock foundation used in the paper. Specifically, ρ_c and ρ_r are the unit weights, E_c and E_r are the elastic moduli, while υ_c and υ_r are the Poisson's ratio; the subscript c indicates the concrete, while r refers to rock. Water is considered to have a unit weight of 1000 kg/m^3, with a compression wave velocity of c_p = 1439 m/s.

The nonlinear behavior of the dam is simulated through the concrete damage plasticity constitutive model, which accounts for both tensile and compressive behavior [36]. This constitutive model has been broadly adopted in structural and dam engineering problems [42] because of its ability to properly capture the response of non-reinforced concrete under cyclic loading. The concrete damage plasticity model requires the definition of the concrete post-elastic behavior, both in compression and in tension, as well as the plastic flow parameters. Specifically, the tensile post-elastic behavior is described through a descending exponential function, while the compressive post-elastic behavior is composed of both a hardening and a softening part [43,44]. The damage to the concrete, due to the development of micro-cracks, is simulated through a reduction of the elastic modulus described by the scalar value d_t as a function of the plastic deformation. Table 2 summarizes the concrete tensile and compressive strength, f_t and f_c, respectively, the fracture energy G_f, as well as the plastic flow parameters adopted in this study [45]. Specifically, Ψ is the dilation angle, ε is the eccentricity that defines the rate at which the flow potential approaches the asymptote, σ_{b0}/σ_{c0} is the ratio of initial equi-biaxial compressive yield stress to initial uniaxial compressive yield stress, and Λ is the ratio of the second stress invariant on the tensile meridian to that on the compressive meridian.

To quantify the damage at different locations and compare among various simulations, a simple damage index concept is used [28] as a ratio of the damaged area to total area, $DI = \frac{\sum_{i=1}^{N_e} A_i \times d_{t,i}}{A_t}$. In this damage index, A_i presents the elemental area, $d_{t,i} \in [0,1]$ is the extent of damage in the element, and A_t is the total area. Since the damage profile and failure mode in brittle materials highly depends on applied seismic excitation, the structure is divided into three regions/zones, and the DI is computed separately in each one. These three regions are shown in Fig. 2 which includes the bottom 20 m (region I), the middle 70 m (region II), and the top 32 m (region III).

4. Signal characteristics and deconvolution

As discussed earlier, the main contribution of this paper is to use a ground motion-compatible IAA in the seismic response of structures. Since this paper is a proof of concept study, the ground motion record recommended by ICOLD [22] is used in all simulations. Taft Lincoln School Tunnel (a.k.a Taft), Kern County, California Earthquake which occurred on July 21, 1952, is used as a target ground motion.[4] Fig. 2(a) illustrates the horizontal component of the acceleration time-series, as well as its acceleration and displacement response spectra at different damping ratios. As seen, this ground motion record has a wavy acceleration spectrum at short periods, i.e., motion at the range 0.2–0.4 s makes IAA optimization a challenging task.

Implementing the procedure discussed in Section 2 yields to a horizontal IAA time series as shown in Fig. 2(b). The acceleration time series is shown along with its envelope, which is zero-period acceleration (ZPA). The ZPA corresponds to PGA in real ground motion records. Although the IAA is not really a ground motion record, throughout this paper the term ZPA is used for all acceleration

[4] The selection of the Taft ground motion is not arbitrary. This specific ground motion record is mandated in the ICOLD benchmark problem and is based on the original work by Chopra in 1988 for the Pine Flat Dam [46]. If one wishes to address the dependency on ground motion, a full IDA simulation using 40 or more ground motion records (for example, those from FEMA P695), would be necessary. This extensive analysis is beyond the scope of this paper and is the topic of a separate study we are currently undertaking.

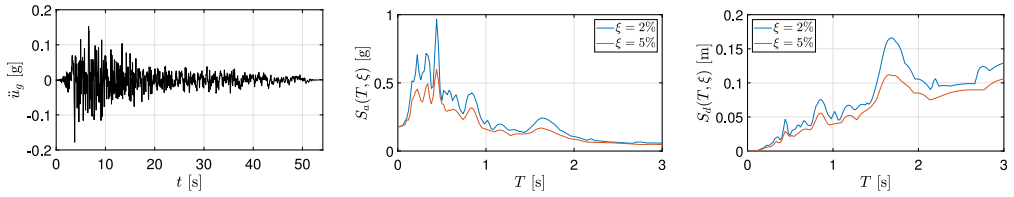

(a) Real ground motion time history

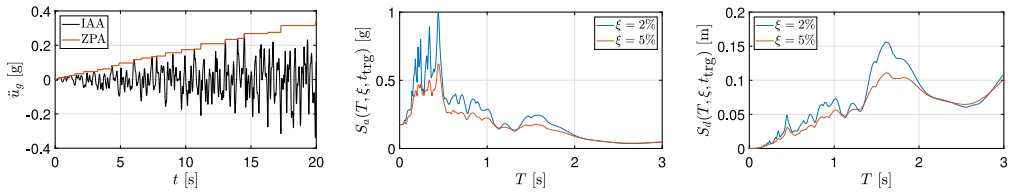

(b) Intensifying artificial acceleration

Fig. 3. Characteristics of the target ground motion record (i.e., Taft record), the IAA, and their response spectra. Note: response spectra for IAA is plotted at target time, 10 s.

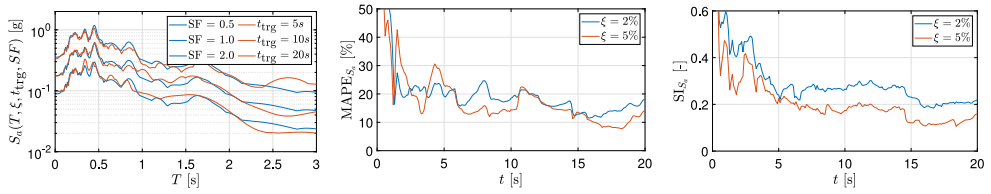

(a) Acceleration response spectra (b) MAPE metric (c) SI metric

Fig. 4. Quantification of error metrics for acceleration response spectra from IAA and target ground motion record at various seismic intensities.

time series to present their maximum absolute value, i.e., $\max(|\ddot{u}|)$. This plot also illustrates the acceleration response spectrum, $S_a(T,\xi,t_{trg})$, and displacement response spectrum, $S_d(T,\xi,t_{trg})$, at the target time of 10 s for two different damping values.

While the acceleration response spectra are already optimized using the objective function in Eq. (1), it is important to quantify the differences for any practical application. Fig. 4(c) compares three sample acceleration response spectra from target ground motion and the corresponding IAA. Three scale factors (SF) of 0.5, 0.1 (original), and 2.0 are used for the target ground motion record. Similarly, three target times of 5, 10, and 20 are used for IAA. Qualitatively, there is a very good match between the response spectra, and the optimized IAA can indeed estimate most of the peak points. To quantify the errors two metrics are used:

$$\text{MAPE} = \frac{1}{N}\sum_{i=1}^{N}\left|\frac{S_a^*(SF_i,T|_0^5) - S_a(t_i,T|_0^5)}{S_a^*(SF_i,T|_0^5)}\right| \times 100\% \tag{5}$$

$$\text{SI} = \frac{\text{RMSE}}{\bar{S}_a^*(SF_i,T|_0^5)}; \quad \text{RMSE} = \left(\frac{1}{N}\sum_{i=1}^{N}\left(S_a^*(SF_i,T|_0^5) - S_a(t_i,T|_0^5)\right)^2\right)^{1/2} \tag{6}$$

where the SF_i and t_i are the ith scale factor (for real ground motion) and target time (for IAA). N is the discretization number, which is assumed to be 200. This means the IAAs are used every 0.1 s (i.e., 20 s/200 = 0.1 s), and the real ground motion is scaled with 0.01 increment (i.e., 0.01:0.01:2.0). The asterisk indicates the response spectra from real ground motion. $\bullet|_0^5$ indicates the evaluation range from zero to five seconds.

Originally, both MAPE (mean absolute percentage error), and SI (scatter index), which is a normalized RMSE (mean root squared error), are dimensionless metrics; however, they can be expressed as percentages for ease of use. Figs. 4(b) and 4(c) present the results for two damping values. Except for the first few seconds of IAA (or the small scale factor of ground motion record), the error metrics are stable. MAPE presents the error of 10%–20% for the majority of comparison domains, while the corresponding value for SI ranges from 0.15–0.30. This confirms that the IAAs are well optimized for the entire seismic intensity domain, and one should expect a consistent structural response from them (this will be discussed in the next section).

In seismic soil/rock-structure interaction analyses, the ground motion record is typically applied at the bottom of the foundation domain. The elastic waves propagate through the elastic rock domain until they reach the top of the foundation. The rock domain acts as a damped filter for the seismic motion, altering the frequency content and amplitudes of the original signal [47]. With reference to Fig. 2, the relationship between the seismic input $\ddot{u}_F(t)$, applied at the bottom of the rock domain, and $\ddot{u}_G(t)$, recorded response in point G, is expressed by the following convolution:

$$\ddot{u}_G(t) = \ddot{u}_F(t) \times h(t), \tag{7}$$

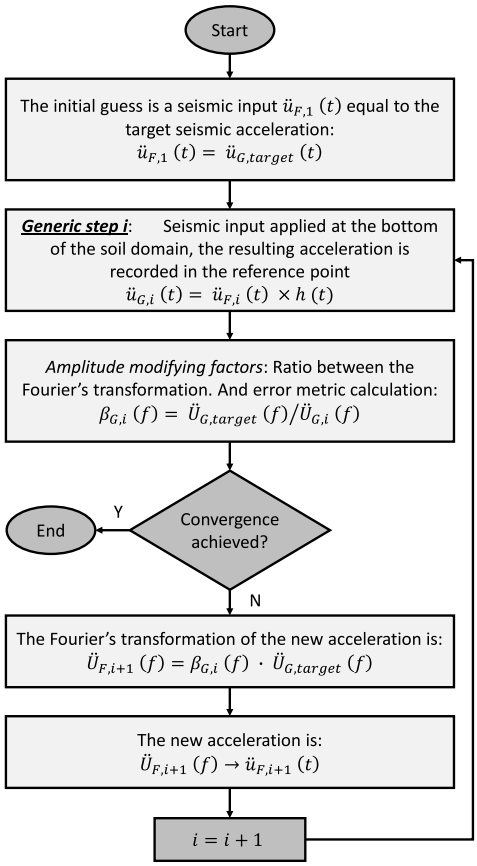

Fig. 5. Applied deconvolution process.

where $h(t)$ is the distortion function of the rock domain acting as a filter.

Therefore, the seismic input applied in point F needs to be deconvolved to have an acceleration in point G matching the target ground motion (or IAA in our case) [48]. The filter distortion $h(t)$ depends on the characteristics of the rock domain, such as the size, elastic properties, and boundary conditions, but also its discretization, number of nodes, and shape function of the finite elements. Given the complexity of the deconvolution problem, a closed-form solution is not typically available. Methods proposed in the scientific literature rely on either approximated solutions or optimization processes [49]. In this paper, a frequency domain optimization process is used. The seismic input applied at the bottom of the dam is optimized to have the Fourier transform of the acceleration recorded in the reference point, i.e., G, matching the Fourier transform of the target seismic motion. The optimization process is shown in Fig. 5. Working in the frequency domain is particularly convenient, and thus, Eq. (7) is re-written as $\ddot{U}_F(f) = \ddot{U}_G(f)/H(f)$, where $\ddot{U}_F(f)$ and $\ddot{U}_G(f)$, are the Fourier transform of the acceleration applied at the bottom of the foundation domain, and the one recorded at the reference point G, respectively, while $H(f)$ is the transfer function.

The optimization process achieves convergence once the Fourier transform of the acceleration recorded in point G matches the Fourier transform of the target seismic input. Fig. 6 shows the comparison between the response spectra of the acceleration recorded at point G at the beginning and the end of the optimization process versus the target seismic input. After a few iterations, the optimization process converges into a solution.

5. Results and discussion

5.1. Validation of FEM with ICOLD benchmark

As discussed in Section 3, this paper adopts the benchmark problem presented and summarized in the 2019 ICOLD workshop [22]. The workshop participants were provided with the detailed geometry, material properties for concrete and rock, and seismic loading. Case "D-3" of the workshop's Theme A consisted of seismic analysis of the case study dam-reservoir-foundation system using the Taft ground motion with the normal water level. The results of the benchmark are compared with those of this paper in terms of acceleration and drift for the linear elastic system with a massless foundation (a comprehensive summary of nonlinear results is not

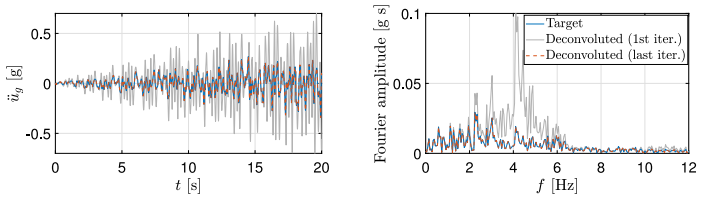

(a) Acceleration time history (b) Fourier amplitude

Fig. 6. Quality of deconvolution process in time and frequency domains.

Table 3
Comparison of median, mean and standard deviation of the benchmark model with the results of this paper.

	Absolute peak horizontal acceleration [g]		Relative crest displacement [m]	
	Heel (point A)	Crest (point C)	Maximum downstream	Minimum upstream
This paper	0.17	1.29	0.060	−0.047
Upper bound	0.24	1.94	0.072	−0.017
Lower bound	0.10	0.50	0.035	−0.076
Mean	0.15	0.89	0.045	−0.032
Standard deviation	0.05	0.47	0.014	+0.020

available). One may note that the variability in the results of participants originates from several factors such as solution algorithm, finite element modeling, software used, boundary conditions, etc.

Table 3 summarizes the statistics of the response quantities collected from benchmark participants, as well as the findings in this paper. It reports the peak horizontal acceleration (PHA) at two index points (i.e., crest and heel), as well as peak relative crest displacement in both positive and negative directions. The PHA is defined as the average absolute value of the minimum and maximum accelerations in a time history, i.e., $\left(\ddot{u}_{max} - \ddot{u}_{min}\right)/2$. Also, the relative crest displacement is computed as a difference between points C and A. According to this table, the benchmark results show a relatively large variation (considering that the geometry and material properties are all provided). The coefficient of variation (COV) for heel and crest PHA is 0.32 and 0.53, respectively. Moreover, the COV for maximum and minimum crest displacement is 0.31 and 0.63, respectively. This table also presents the results of modeling in this paper, and as seen they are close to mean responses, typically falling within the range "mean ± one standard deviation". Therefore, we can use this model with good confidence for subsequent comparisons between IDA and IAA. The recorded PHA at heel point A is in good agreement with the mean of the benchmark. However, the crest point C shows a bit more discrepancy. This means that the wave has properly traveled through the foundation medium; however, depending on the damping value/mechanism, the super-structure may exhibit different responses.

5.2. IAA vs. Single-record IDA

Having a calibrated finite element model, it is used to conduct multiple transient simulations using the real ground motion and the generated IAA. As discussed earlier in Fig. 1, the main objective of this paper is to validate IAA performance with respect to its single-record IDA. This paper considers two distinct scenarios to broaden the applicability of its results: (1) nonlinear damage model with massless foundation (i.e., no wave propagation and no deconvolution process), and (2) nonlinear damage model with massed foundation (i.e., wave propagation is included and deconvolution is needed). It is important to note that the initial phase of simulations, which do not exhibit crack formation, effectively corresponds to linear models.

The IDA method has been originally developed for nonlinear structures [3] in which the scale factor of the ground motion record is incrementally increased until the numerical model indicates failure. While the scale factor can be increased by constant increments (i.e., the easier way), there are other alternatives such as hunt&fill method [3], which optimizes this process (i.e., the smarter way). For both nonlinear models, the hunt&fill method is used in this paper to conduct the IDA. In both cases, a total of ten transient simulations were required. Therefore, each model in this paper was analyzed 11 times (10 simulations for IDA with 10 scaled records, and one IAA). A classical IDA curve is developed by connecting all the peak responses from different scaled records and plotting them versus the seismic intensity of the scaled record. There exist multiple alternatives to connect the discrete data points from IDA such as piecewise linear interpolation, spline interpolation, or the Ramberg–Osgood equation [50]. In this paper, we use the simple linear interpolation method. This curve which presents the relationship between the engineering demand parameter (EDP) and the seismic intensity measure (IM) parameter is typically called a capacity function.

On the other hand, generating the capacity function based on IAA has a completely different procedure. First, the response time history (e.g., displacement) is recorded, i.e., EDP(t). It should be noted that in nonlinear systems, the analysis might terminate prematurely at a certain time, t_{fail}, due to either numerical non-convergence or physical failure conditions, such as exceeding a specified drift threshold. Next, the maximum value of the absolute EDP is computed at any time τ using the following operator:

$$\Omega(EDP(t)) = \max\left(|EDP(\tau)|\right); \quad \tau \in [0, t] \tag{8}$$

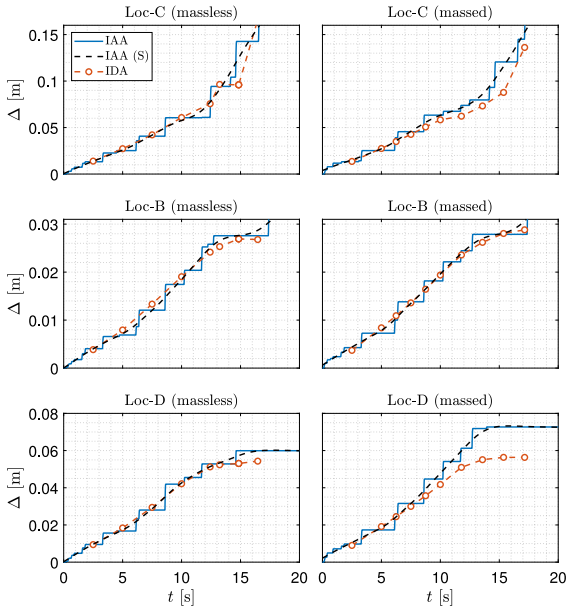

Fig. 7. Comparison of peak displacement from IAA and IDA at three locations and four modeling scenarios.

The product of this step is a step-wise increasing function in the EDP-time coordinate system. To compare the results with those from IDA, they both should have the same coordinate system. Therefore, the "time" parameter in IAA needs to be converted into an appropriate IM parameter. This is indeed an iterative procedure in which the truncated acceleration at any time interval $[0, \tau]$ should be used to compute the IM parameter. The final product is a step-wise capacity function in the EDP-IM coordinate system and can be compared to that from IDA. The rest of this section presents the EDP-time results (in Fig. 7), IM-time results (in Fig. 8), and the EDP-IM capacity functions (in Figs. 9 and 10(a)).

Fig. 7 presents the peak displacement at three different locations of the crest (point C), upstream face mid-height (point B), and downstream neck discontinuity (point D), and for two modeling scenarios. The results for IAA are presented in the EDP-time coordinate system, and the IDA curve is converted into the "time" domain. The scale factor for each of the simulations in IDA is converted into equivalent time as $t_{SF} = 10 \times SF$ [s] (note that 10 s is the target time discussed in Eq. (2)). There is a reasonable consistency between the capacity curves from IAA and IDA (in the time domain). Both modeling assumptions provide an exact prediction of displacement response at the target time, i.e., 10 s. The IAA-based curves can identify the nonlinearity in the system precisely. Both the starting point of the nonlinear curve, and its degree (i.e., curvature) are predicted well. For crest displacement (point C), the capacity curves are concave up, while for the lower elevation points, it has a concave down behavior. This means that progressing the IAA simulation from 12 to 16 s causes significant damage to the upper portions of the dam. Similar behavior is observed in IDA for the scale factor from 1.2 to 1.6.

It is noteworthy that the quality of the comparison between IAA and IDA also depends on the selected point. Point C, located at the top left of the model, provides a global response and in most cases is not sensitive to the details of crack propagation in the dam body. Point B, located in the upstream mid-height, provides the response variation for the bottom half of the dam and is mainly sensitive to dam-foundation cracking. Point D, located in the downstream neck, can be sensitive to crack initiation and propagation at the neck, which is often one of the failure modes. Therefore, a slightly different location of crack initiation (one element above or below this point) can significantly affect the displacement at this point. The slight mismatch observed in the last 10 s of the massed foundation model at location D in Fig. 7 can be attributed to variations in the crack development process. Yet, it is evident that such local differences do not translate into the global response at Point C.

Fig. 8 illustrates the absolute peak acceleration at three different locations: the bottom of the foundation domain (point F), the foundation free-surface away from the dam (point G), and the foundation free-surface next to the structure (point A). These three locations were selected to investigate the accuracy of acceleration estimation under different conditions. Again, the general consistency between IAA and IDA is satisfactory for all modeling assumptions.

Fig. 9 combines the results of Figs. 7 and 8 to develop the EDP-IM capacity functions. The EDP is chosen to be the crest relative displacement (point C), while three alternative IM parameters are examined to find the optimal one (all based on the recordings at point G), including zero-period acceleration (equivalent to PGA), first-mode spectral acceleration, $S_a(T_1)$, and normalized spectral acceleration at the period range of $[\alpha T_1, \beta T_1]$ (the lower and upper bound of the period are assumed to be 0.2 and 2 s, respectively). The latter scenario averages the spectral acceleration over a specified period range. While $S_a(T_1)$ accounts for the spectral value (which is typically proven to be a better IM parameter compared to PGA [51]), the $\bar{S}_a^{[\alpha,\beta]}(T_1)$ also considers the spectral shape.

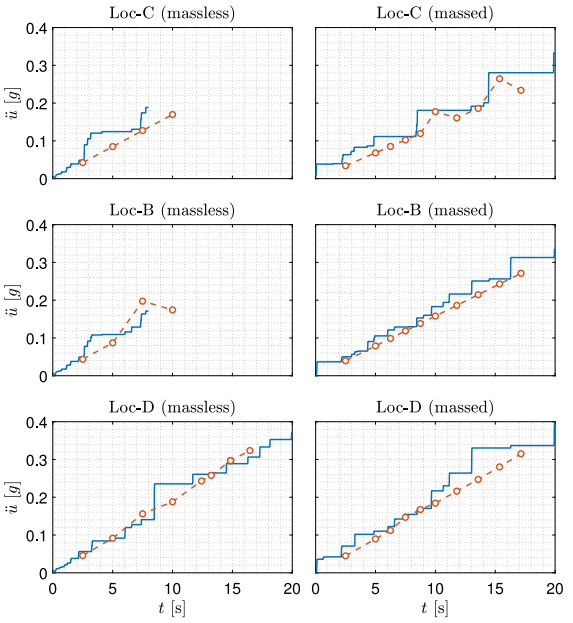

Fig. 8. Comparison of absolute peak recorded accelerations from IAA and IDA at three locations within the foundation for four modeling scenarios.

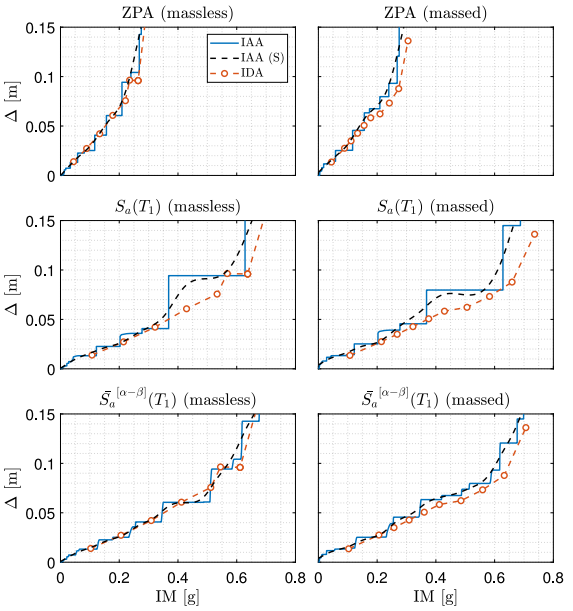

Fig. 9. Direct comparison IAA and IDA in terms of various IM parameters and a global EDP (i.e., displacement).

This is particularly effective for nonlinear systems in which the potential damage shifts the period of the system towards a larger value (i.e., the damage makes the system more flexible) [52]. There exist many other alternatives to be used as IM parameters that are ignored in this paper. A full list can be found in [53,54]. For all three IM parameters, we observed reasonable compatibility between IDA and IAA capacity functions. Using $S_a(T_1)$ causes large steps in IAA, which leads to deviation of its capacity function from IDA at some intensity ranges. However, $\bar{S}_a^{[\alpha,\beta]}(T_1)$ solves this problem and returns a very smoothed capacity function for IAA. More specifically, the IAA can precisely estimate the onset of nonlinearity in capacity function and follows the same trend as IDA.

All the comparisons between IDA and IAA were limited to peak response estimation. This is indeed, the goal of the IAA. Some internal features in the IAA may not match exactly the corresponding IDA. However, this does not affect the primary purpose of the IAA. For example, the number of stress cycles beyond a threshold might be different between IAA and IDA. According to Fig. 3, the duration of the real ground motion is about 54 s, while the IAA is only 20 s. Therefore, the real ground motion includes more

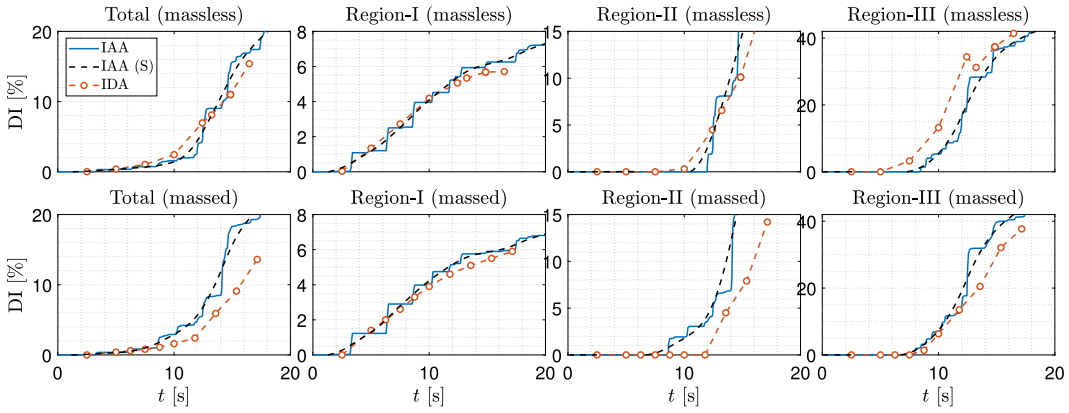

(a) Comparison of damage index from IAA and IDA for two nonlinear finite element models

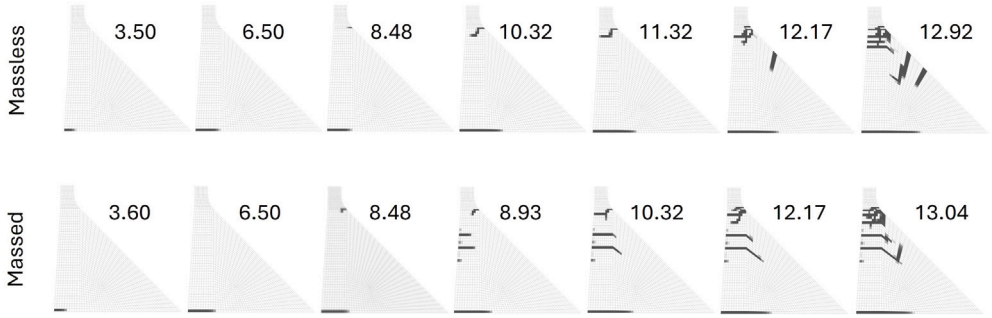

(b) Comparison of crack profiles at different time instance (s)

Fig. 10. Evaluating the damage response of dam in terms of damage index and crack propagation.

cycles than the IAA. The US Army Corps of Engineers [55] recommends checking the number of effective stress cycles in the linear elastic analysis of dams as an indicator for potential damage in the nonlinear models.

One may argue that the ground motion duration and stress cycles are indeed more effective in nonlinear systems compared to the linear elastic ones. Fig. 10(a) compares the damage index in three main regions (i.e., lower, middle, and upper parts), as well as the entire structure. The DI in region-I is nearly identical between IDA and IAA. The IAA can even estimate the concave-down nature of the DI curve. The DI is also close in region-II and III between IDA and IAA, and in general, 0%–20% differences can be observed. Finally, the total DI from the massless foundation model is nearly matched, while the one from massed foundation model has up to 15% differences. In all cases, the IAA well estimates the time (or seismic intensity) which corresponds to the initiation of the damage. From an engineering perspective, this is a reasonably well match between IDA and IAA. So, regardless of cumulative inelastic duration (and the number of potential stress cycles), the IAA well predicts the results of IDA. Moreover, Fig. 10(b) demonstrates the progression of crack propagation at various times for two nonlinear models under IAA loading. Initial observations indicate minor differences in damage extent at earlier stages, but distinct crack paths become evident at later times. Notably, aside from the principal crack at the base and neck, additional crack trajectories predominantly form on the downstream face of the dam when considering a massless foundation model. Conversely, with a massed foundation model, crack initiation and expansion are observed to commence from the upstream side.

Another consideration in nonlinear seismic analysis of concrete dams is to determine the collapse. This is typically considered in numerical simulations using two criteria: (1) reaching the collapse limit state, or (2) encountering numerical instability due to very large deformations. Unlike framed structures, which have predefined thresholds for different limit states (e.g., 5% drift ratio for reinforced concrete frames in collapse level), there is no codified threshold for mass concrete dams. Some research papers have proposed drift limits for concrete gravity dams, including Hariri-Ardebili and Saouma [29], who suggested using a 0.1% drift ratio based on prior work by Ellingwood and Tekie [56] and Zhong et al. [57]. Another criterion to identify collapse in concrete dams is the observation of a through crack within the cross-section. This means that a continuous crack path forms, connecting the upstream to the downstream side. Even in the case of a through crack, catastrophic failure occurs when there is large deformation in part of the structure, corresponding to the uncontrolled release of the reservoir.

For Pine Flat Dam, the 0.1% drift ratio is equal to 0.122 m. For the massless foundation model assumption, this criterion is reached at about 15 s of IAA duration, while for the massed foundation assumption, the corresponding failure time is about 16 s (see Fig. 7). Tracking the failure ZPA in Fig. 9 shows values of about 0.25 g and 0.3 g for the massless and massed foundation model assumptions, respectively. Similar $S_a(T_1)$ failure values are 0.6–0.65 g for the massless model and 0.65–0.70 g for the massed

foundation model. In all cases, the IAA estimated failure time or intensity measure is in very good agreement with respect to the IDA method, with an error percentage of less than 10%. It is noteworthy that using a combined intensity measure parameter, i.e., $\bar{S}_a^{[\alpha,\beta]}(T_1)$, reduces the failure intensity estimation error to less than 5%.

In the development of IAAs, a bilinear elasto-plastic model was employed to define the force–displacement relationship. This model was chosen for its simplicity and wide applicability to various structural systems. Although alternative nonlinear models that elaborate on cyclic stiffness and strength degradation exist [58], their incorporation would significantly increase the number of design optimization variables, potentially complicating the optimization process with increased complexity and computational demands. It has been shown in this study that a simplification to the nonlinear force–displacement relationship in IAAs reasonably matches the outcomes observed with the concrete damage plasticity model, which utilizes plasticity theory for compressive loads and damage mechanics theory to account for the degradation of material stiffness due to microcracking under both tension and compression. Additionally, a study by Hariri-Ardebili and Sattar [59] revealed that the choice among such modeling variations may not significantly affect the overall fragility estimates, particularly with the use of generic IAAs rather than ground motion-specific IAAs. Therefore, to maintain a balance between model fidelity and the feasibility of optimization, the bilinear model was deemed the most appropriate choice for this analysis.

6. Discussion: Integration in risk framework

This paper has presented a systematic framework for generating IAAs that are compatible with a specific real ground motion record. This compatibility extends to various scales of the original ground motion as examined through IDA. A detailed application of this methodology has been demonstrated on a complex engineering structure, encompassing a coupled dam-water-foundation system across both linear and nonlinear ranges, under varying wave propagation assumptions.

Assuming the applicability of ground motion-compatible IAAs across general engineering problems, an important consideration is how this method can be integrated within current risk assessment practices. This section proposes a conceptual framing for such integration.

A primary application of ground motion-specific IAAs is within the Performance-Based Earthquake Engineering (PBEE) framework [60], which is structured around several key phases: seismic hazard analysis, structural response analysis, damage analysis, and loss assessment. Each phase generates critical variables, namely the intensity measure (IM), engineering demand parameter (EDP), damage measure (DM), and decision variable (DV), which are interconnected through the total probability theorem [61]:

$$\lambda_{\mathrm{DV}}(dv) = \int_{dm}\int_{edp}\int_{im} G_{\mathrm{DV|DM}}[dv|dm]\left|\mathrm{d}G_{\mathrm{DM|EDP}}[dm|edp]\right|\left|\mathrm{d}G_{\mathrm{EDP|IM}}[edp|im]\right|\left|\mathrm{d}\lambda_{\mathrm{IM}}(im)\right| \tag{9}$$

where $G_{\mathrm{X|Y}}[x|y] = P\left[\mathrm{X} > x|\mathrm{Y} = y\right]$ represents the conditional complementary cumulative distribution function of the random variable (RV) X given Y = y.

Employing ground motion-compatible IAAs could benefit different components of PBEE. For instance, in the event of a seismic hazard analysis updating the ground motion set, this framework facilitates the completion of all required simulations efficiently. Fig. 11 depicts a conceptual model for risk analysis that integrates IAA, defining risk as a product of hazard, vulnerability, and exposure. The proposed framework inserts itself, and may bring enhancements, in two phases: (1) following hazard analysis selection of ground motions, corresponding IAAs are generated for use in structural simulations; (2) IAA-derived capacity curves are then processed as outlined in this study to produce the conventional IM-EDP relationship (e.g., $S_a(T_1) - \Delta_{max}$). Subsequently, the process progresses as usual to develop fragility curves capturing the variability of ground motion RTR.

Incorporating material and modeling uncertainties into IAA-based assessment requires additional steps. There are two broad approaches to address this issue: (1) utilizing recommended values from the literature, and (2) performing direct simulations. In the first approach, analysts minimize efforts by using recommended logarithmic standard deviation or coefficient of variation values for different sources of material and modeling randomness. For example, Hariri-Ardebili [34] recommends a modeling-related dispersion value of 0.45 for maximum dynamic crest displacement, 0.30 for maximum hydrodynamic pressure at the heel, 0.32 for heel maximum acceleration, and 0.30 for crest maximum acceleration. Several studies consider material-related uncertainties, such as the randomness in concrete properties like elasticity, strength, and concrete-rock joint properties [62–66].

In the second approach, analysts perform direct simulations to quantify epistemic-type uncertainty sources. Material and modeling randomness are accounted for using probabilistic simulation-based techniques such as Latin Hypercube Sampling (typically for material randomness) and full/partial factorial design (typically for modeling randomness). In this approach, a total of N_{sim} samples of the finite element model, representing the entire space of specified random variables, are prepared. Each sample is then subjected to the target IAA, resulting in N_{sim} response curves that represent the epistemic variability under the target IAA. This method has been discussed for structural components [67], but the same technique is applicable to dams and other infrastructures. When more than one IAA (associated with different ground motion records) is combined with N_{sim} model samples, both aleatory and epistemic uncertainties are addressed simultaneously. This approach is similar to the extended incremental dynamic analysis (EIDA) as discussed by Dolšek [68].

Within the PBEE framework, three principal decision variables gauge the performance of structural systems: direct monetary loss, downtime, and fatalities. These assessments hinge on risk evaluations for different damage states. The annual likelihood of exceedance of a damage state, as defined by a specific fragility function, is determined by the following formula:

$$\lambda_{ds} = \int_{im=0}^{\infty} \mathbb{P}[\mathrm{DS} > ds_i|\mathrm{IM} = im]\cdot\left|\frac{d\lambda_{\mathrm{IM}}(im)}{d(im)}\right| d(im) \tag{10}$$

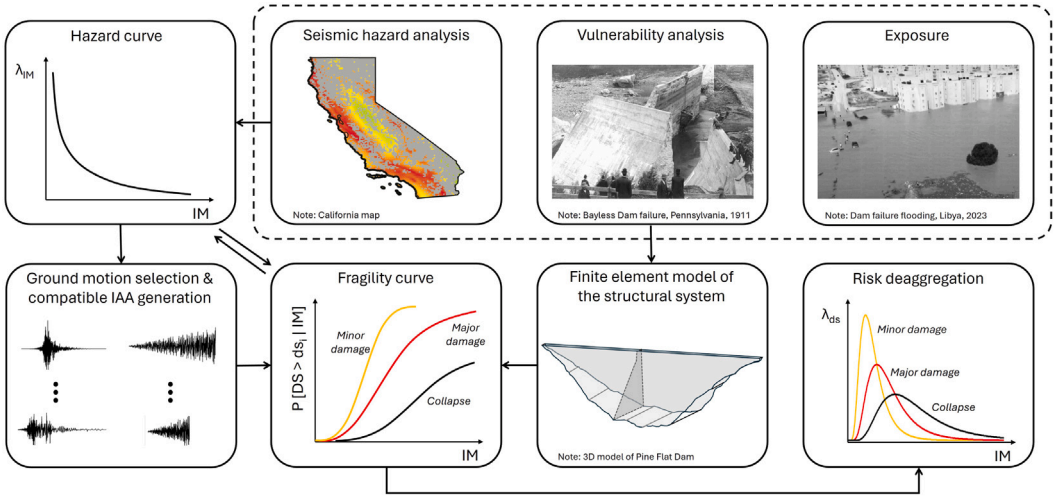

Fig. 11. A conceptual framework for risk analysis incorporating IAA.

Here, $\mathbb{P}[DS > ds_i|IM = im]$ denotes the likelihood of the structure surpassing a given damage state i (i.e., the fragility curve), λ_{IM} represents the annual frequency of ground motions exceeding intensity measure IM, and $\left|\frac{d\lambda_{IM}(im)}{d(im)}\right|$ indicates the gradient of the hazard curve, reflecting the rate of change in ground motion frequency as a function of the intensity measure.

One of the most resource-intensive tasks for structural engineers dealing with PBEE is in fact performing the probabilistic nonlinear dynamic analyses of numerical models required when assessing the vulnerability of complex structures. Traditional frameworks typically rely on methods such as IDA, MSA, or CLA to derive probabilistic outcomes. However, by generating ground motion-compatible IAAs for a set of ground motions derived from hazard analysis, a significantly reduced number of simulations are needed to replicate the RTR variability of ground motion. For instance, with an initial set of 40 ground motion records (e.g., the FEMA P695 series), an IAA compatible with each record can be developed. Consequently, only 40 nonlinear transient simulations would be necessary to construct or replicate the multi-record IDA. This approach may significantly streamline the development of high-fidelity fragility curves for critical structures, traditionally a time-consuming endeavor, and therefore aid in the practical application of PBEE.

Fig. 12 illustrates the application of the proposed framework to the Pine Flat Dam. The seismic hazard curve is obtained from the USGS seismic hazard tools for two IMs: zero-period acceleration and spectral acceleration at the fundamental period of the dam, as shown in Fig. 12(a). It is important to note that the USGS tool provides hazard data for a limited set of predefined periods. If the fundamental period of the system does not match these predefined values, interpolation is required to estimate the hazard at the desired period. Similarly, when employing a parameter such as $\bar{S}_a^{[\alpha,\beta]}(T_1)$ as the IM, interpolation is also necessary.

Next, fragility curves are developed using 12 ground-motion-compatible IAAs generated for the dam. These 12 records represent the minimum number of simulations commonly cited in the literature [69] for Pine Flat Dam. While a detailed comparison of these IAAs with IDA is beyond the scope of this paper, such comparisons will be addressed in subsequent publications. The smoothed IAA curves are utilized to derive fragility estimates, as detailed in prior studies [70]. For consistency in this paper, a single limit state is considered, defined as a 0.1% drift ratio corresponding to theoretical failure [29,56,57]. Based on this assumption, a median seismic capacity of 0.61 g and a logarithmic standard deviation of 0.38 g are computed. This dispersion value is consistent with the typically recommended value of 0.4 g and aligns with previous studies on the fragility analysis of concrete dams [71]. At this stage, the uncertainty analysis incorporates only the ground motion RTR variability.

As discussed earlier, additional sources of uncertainty – specifically material and modeling variability – can be incorporated using a simplified square root of the sum of squares (SRSS) method. Material and modeling uncertainties are assumed to have standard deviations of 0.35 g and 0.45 g, respectively. Fig. 12(b) presents four variations of fragility curves, each considering one, two, or all three sources of uncertainty.

By integrating the hazard and fragility curves, risk deaggregation plots are generated, as shown in Fig. 12(c). These plots reveal that seismic intensities of 1.0 g or less contribute most significantly to the total risk. Furthermore, the results demonstrate that incorporating additional sources of uncertainty substantially increases the total risk. The total risk, represented by the area under the risk deaggregation curves, is summarized in Fig. 12(d). This figure quantifies the total risk and highlights the relative importance of different uncertainty levels.

7. Conclusions

Seismic risk analysis typically covers the progressive failure assessment of structural and infrastructural systems, which also includes the uncertainty quantification in various aspects of modeling, simulation, and loading protocols. Such an effort in

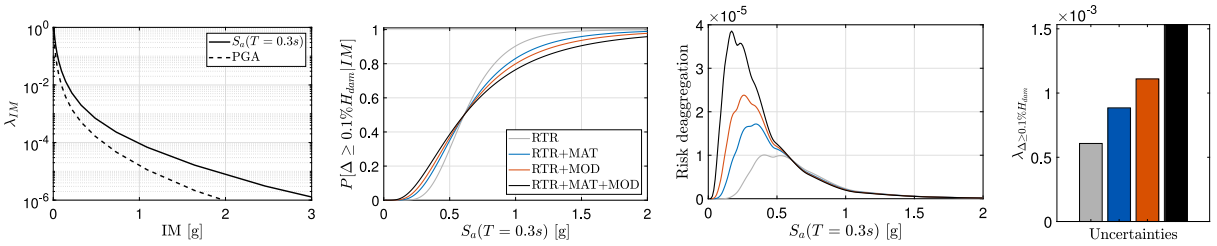

(a) Hazard curves (b) Fragility curves (c) Risk curves (d) Total risk

Fig. 12. Risk assessment of Pine Flat Dam model with different level of uncertainties.

earthquake engineering is coupled with performing probabilistic simulations and accounting for randomness in ground motion selection and scaling, modeling, and material randomnesses. As much as the outcome from such probabilistic simulations is informative, it is computationally expensive too. While performing thousands of transient simulations might be doable for simple framed structures, it is practically impossible for complex infrastructures like bridges, nuclear power plants, tunnels, and dams.

Therefore, this paper proposed the intensifying artificial acceleration (IAA) as an alternative technique used to estimate the seismic response of structures. The IAA estimates the seismic response of the structures from linear elastic range to nonlinear range, and finally the collapse limit state. This paper addressed two main questions regarding the application of IAA: (1) its agreement with respect to single-record incremental dynamic analysis (IDA), and (2) different soil/rock-structure modeling assumptions. While the detailed results have been discussed in the paper, the following are general conclusions and future works:

- Overall, the generated ground motion-compatible IAA is capable of estimating the seismic response of a complex structural system with reasonable accuracy. Various modeling assumptions are compared including the linear and nonlinear responses, and also the massed and massless foundation models.
- For the massed foundation systems, a deconvolution process is typically required to obtain the seismic motion at the bottom of the bedrock. The IAA is deconvolutable and provides a reasonable estimation similar to the deconvolved real ground motion record.
- Comparison of single-record IDA and IAA results is possible in both EDP-time or EDP-IM coordinate systems. In both cases, the key is to use an appropriate conversion between the time and IM parameter. Among many alternatives, the zero-period acceleration, first-mode spectral acceleration, and the mean spectral acceleration at a period range of 0.2–2 of the T_1 were examined. It is found all are acceptable, while the latter one is optimal as it created a smoother IAA capacity function. One may note that for regional risk assessment, the zero-period acceleration is a hazard-consistent intensity measure.
- The IAA-based capacity function is capable of estimating both the global (e.g., displacement) and local (e.g., stress and crack) EDPs. Although the number of stress cycles might be different between the IAA and specially the scaled ground motion records, this may not have a significant impact on the damage response, as the damage index from IAA matches with those obtained from IDA. The development of cracks is sensitive to small variations of the input excitation. The highest discrepancy is observed in the middle body, while the damage indices at the base and neck areas are very close.

Given the reasonable match between IAA and single-record IDA outcomes, the introduced framework offers notable computational efficiency benefits. Despite the initial computational expense incurred during the generation of ground motion-compatible IAA, this cost is markedly less than that of conducting multiple transient simulations in IDA. For a nonlinear deterministic model, IAA can achieve a reduction of approximately 90% in the number of required simulations compared to IDA for each ground motion record (assuming that typically around 10 simulations are required in IDA for each ground motion record), with even greater savings in actual wall clock time. This improvement is attributed to three key factors related to loading and solution processes. (1) Increment count: Typical ground motion records, such as those in the FEMA P695 far-field set, span 30–100 s with a sampling rate of 0.005 s (or 0.01 s for older recordings), necessitating 3,000 to 20,000 increments per simulation. In contrast, IAAs require only about 2,000 increments, substantially reducing the total computation time. (2) Iteration requirements at high seismic intensities: As the model enters its nonlinear response phase under high seismic intensities, additional iterations within each increment are needed to achieve convergence. (3) Strategic activation of nonlinear mechanisms in IAA: The IAA design focuses on activating the structure's nonlinear mechanisms towards the end of the loading sequence. This approach contrasts with typical ground motion records where peak loads often occur in the first half of the duration. Consequently, if nonlinear mechanisms are triggered at peak loading, the system does not revert to a linear response in post-peak phases, despite a reduction in loading intensity. Damage, manifesting as cracking, yielding, or other material degradations, irreversibly alters material properties and structural stiffness. This necessitates in real ground motions a higher proportion of increments to undergo additional iterations to meet convergence criteria, further emphasizing IAA's computational advantage.

Although this paper provided very detailed results on the comparison of the single-record IDA and its compatible IAA, further research is required to validate other ground motion records, other types of structural systems, and modeling assumptions. The studies should also be expanded to various types of foundation properties with different shear wave velocities, and probably with different layers of rock material properties. For future studies, the impact of the multi-component ground motion record should be evaluated as well. The proposed framework in this paper should be expanded for the multi-record IDA and the fragility functions

derived from IDA and IAA need to be validated. Once all these requirements are fulfilled, the proposed IAA-based performance evaluation can be considered as an alternative to other probabilistic structural simulation methods to be used in the context of the PBEE.

CRediT authorship contribution statement

M. Amin Hariri-Ardebili: Writing – review & editing, Writing – original draft, Visualization, Validation, Supervision, Software, Resources, Project administration, Methodology, Formal analysis, Conceptualization. **Giacomo Sevieri:** Writing – review & editing, Writing – original draft, Validation, Software, Resources, Methodology, Formal analysis. **Carlo Resta:** Writing – review & editing, Writing – original draft, Validation, Software, Resources, Methodology, Formal analysis. **Anna De Falco:** Writing – review & editing, Validation, Resources, Methodology. **Sissy Nikolaou:** Writing – review & editing, Validation, Project administration, Methodology, Conceptualization. **Siamak Sattar:** Writing – review & editing, Validation, Project administration, Methodology, Conceptualization.

Disclaimer

Certain commercial equipment, instruments, or materials are identified in this paper to foster understanding. Such identification does not imply recommendation or endorsement by the National Institute of Standards and Technology, nor does it imply that the materials or equipment identified are necessarily the best available for the purpose.

Declaration of competing interest

The authors declare that they have no known competing financial interests or personal relationships that could have appeared to influence the work reported in this paper.

Acknowledgments

This work was supported by the National Institute of Standards and Technology (NIST), USA. Dr. Amin Hariri was supported through PREP, USA agreement no. 70NANB23H024 between NIST and the University of Maryland, College Park. The authors would like to thank Dr. Salamon, Dr. Estekanchi, and Dr. Mashayekhi for their contributions to some aspects of this research.

Data availability

Data will be made available on request.

References

[1] V.E. Saouma, M.A. Hariri-Ardebili, Aging, Shaking, and Cracking of Infrastructures: From Mechanics to Concrete Dams and Nuclear Structures, Springer, 2021.
[2] USACE, Earthquake Design and Evaluation of Concrete Hydraulic Structures, Technical Report EM 1110-2-6053, Department of the Army, U.S. Army Corps of Engineers, Washington D.C., USA, 2007.
[3] D. Vamvatsikos, C. Cornell, Incremental dynamic analysis, Earthq. Eng. Struct. Dyn. 31 (2002) 491–514.
[4] A. Miano, F. Jalayer, H. Ebrahimian, A. Prota, Cloud to IDA: Efficient fragility assessment with limited scaling, Earthq. Eng. Struct. Dyn. 47 (5) (2018) 1124–1147.
[5] K. Mackie, B. Stojadinovic, Comparison of incremental dynamic, cloud, and stripe methods for computing probabilistic seismic demand models, in: Proceedings of the 2005 Structures Congress and the 2005 Forensic Engineering Symposium, New York, NY, 2005, pp. 1–11.
[6] H. Estekanchi, V. Valamanesh, A. Vafai, Application of endurance time method in linear seismic analysis, Eng. Struct. 29 (10) (2007) 2551–2562.
[7] M.A. Hariri-Ardebili, S. Sattar, Myths and realities about ETA, Ocean Eng. 221 (2021) 108499.
[8] H.E. Estekanchi, H.A. Vafai, Seismic Analysis and Design Using the Endurance Time Method, CRC Press, 2021.
[9] H.E. Estekanchi, M. Mashayekhi, H. Vafai, G. Ahmadi, S.A. Mirfarhadi, M. Harati, A state-of-knowledge review on the endurance time method, Structures 27 (2020) 2288–2299.
[10] A. Nozari, H. Estekanchi, Optimization of endurance time acceleration functions for seismic assessment of structures, Int. J. Optim. Civ. Eng. 1 (2011) 257–277.
[11] American Society of Mechanical Engineers, Guide for Verification and Validation in Computational Solid Mechanics, ASME, 2006.
[12] M. Mashayekhi, H. Estekanchi, H. Vafai, S.A. Mirfarhadi, Development of hysteretic energy compatible endurance time excitations and its application, Eng. Struct. 177 (2018) 753–769.
[13] M. Mashayekhi, H. Estekanchi, A. Vafai, S.A. Mirfarhadi, Simulation of cumulative absolute velocity consistent endurance time excitations, J. Earthq. Eng. (2018) 1–26.
[14] Y. Pang, L. Cai, W. He, L. Wu, Seismic assessment of deep water bridges in reservoir considering hydrodynamic effects using endurance time analysis, Ocean Eng. 198 (2020) 106846.
[15] S. Li, K. Liu, X. Liu, C. Zhai, F. Xie, Efficient structural seismic performance evaluation method using improved endurance time analysis, Earthq. Eng. Eng. Vib. 18 (4) (2019) 795–809.
[16] R. Zhang, L. Zhang, C. Pan, Q. Chen, Y. Wang, Generating high spectral consistent endurance time excitations by a modified time-domain spectral matching method, Soil Dyn. Earthq. Eng. 145 (2021) 106708.
[17] M. Mashayekhi, H. Estekanchi, Investigation of strong-motion duration consistency in endurance time excitation functions, Sci. Iranica 20 (2013) 1085–1093.
[18] F. Turchetti, E. Tubaldi, E. Patelli, P. Castaldo, C. Málaga-Chuquitaype, Damage modelling of a bridge pier subjected to multiple earthquakes: a comparative study, Bull. Earthq. Eng. 21 (9) (2023) 4541–4564.

[19] M.A. Hariri-Ardebili, H. Tosun, Dams in the wake-up call of the 2023 türkiye earthquake sequence: Insights from observed damages, risk assessment, and monitoring, Int. J. Disaster Risk Reduct. 102 (2024) 104284.
[20] A.H. Farivarrad, H.E. Estekanchi, Seismic performance assessment of SMRF structures subjected to mainshock-aftershock seismic sequences by endurance time method, J. Earthq. Eng. 26 (7) (2022) 3281–3299.
[21] J. Salamon, Evaluation of Numerical Models and Input Parameters in the Analysis of Concrete Dams, Technical Report DSO-19-13, U.S. Bureau of Reclamation, Denver, Colorado, 2018.
[22] J. Salamon, C. Wood, M.A. Hariri-Ardebili, R. Malm, G. Faggiani, Seismic analysis of pine flat concrete dam: formulation and synthesis of results, in: ICOLD International Benchmark Workshop on Numerical Analysis of Dams, ICOLD-BW, Springer, 2019, pp. 3–97.
[23] D. Rea, C. Liaw, A.K. Chopra, Dynamic Properties of Pine Flat Dam, Technical Report, CALIFORNIA UNIV BERKELEY EARTHQUAKE ENGINEERING RESEARCH CENTER, 1972.
[24] A.K. Chopra, P. Chakrabarti, S. Gupta, Earthquake Response of Concrete Gravity Dams Including Hydrodynamic and Foundation Interaction Effects, Technical Report, CALIFORNIA UNIV BERKELEY EARTHQUAKE ENGINEERING RESEARCH CENTER, 1980.
[25] J.W. Chávez, G. Fenves, Earthquake response of concrete gravity dams including base sliding, J. Struct. Eng. 121 (5) (1995) 865–875.
[26] G. Fenves, A. Chopra, Simplified Analysis for Earthquake Resistant Design of Concrete Gravity Dams, Technical Report UCB/EERC-85/10, Earthquake Engineering Research Center, Berkeley, CA, 1986.
[27] M.A. Hariri-Ardebili, H. Mirzabozorg, Estimation of probable damages in arch dams subjected to strong ground motions using endurance time acceleration functions, KSCE J. Civ. Eng. 18 (2014) 574–586.
[28] M.A. Hariri-Ardebili, L. Furgani, M. Meghella, V. Saouma, A new class of seismic damage and performance indices for arch dams via ETA method, Eng. Struct. 110 (2016) 145–160.
[29] M.A. Hariri-Ardebili, V. Saouma, Quantitative failure metric for gravity dams, Earthq. Eng. Struct. Dyn. 44 (2015) 461–480.
[30] G. Bolzon, D. Sterpi, G. Mazza, A. Frigerio, Numerical analysis of dams, in: Proceedings of the 15th ICOLD International Benchmark Workshop, Springer, 2019.
[31] C. Liang, J. Chen, Q. Xu, J. Li, Correlation study between seismic intensity measures and nonlinear response of arch dam via endurance time analysis, KSCE J. Civ. Eng. 25 (1) (2021) 256–271.
[32] Q. Xu, S. Xu, J. Chen, J. Li, A modified endurance time analysis algorithm to correct duration effects for a concrete gravity dam, Int. J. Geomech. 22 (2) (2022) 04021285.
[33] Q. Xu, T. Zhang, J. Chen, J. Li, C. Li, The influence of reinforcement strengthening on seismic response and index correlation for high arch dams by endurance time analysis method, in: Structures, Vol. 32, Elsevier, 2021, pp. 355–379.
[34] M.A. Hariri-Ardebili, Quantifying modeling uncertainties in seismic analysis of dams: Insights from an international benchmark study, Earthq. Eng. Struct. Dyn. (2024).
[35] ABAQUS, ABAQUS Version 6.14 - Documentation manual, 2014.
[36] J. Lee, G.L. Fenves, Plastic-damage model for cyclic loading of concrete structures, J. Eng. Mech. 124 (8) (1998) 892–900.
[37] A. De Falco, M. Mori, G. Sevieri, Simplified soil-structure interaction models for concrete gravity dams, in: Proceedings of the 6th European Conference on Computational Mechanics (ECCM 6) and the 7th European Conference on Computational Fluid Dynamics (ECFD 7), 2018, pp. 2269–2280.
[38] A. Løkke, A. Chopra, Direct finite element method for nonlinear earthquake analysis of concrete dams: Simplification, modeling, and practical application, Earthq. Eng. Struct. Dyn. 48 (2019) 818–842.
[39] E. Wilson, Three-Dimensional Static and Dynamic Analysis of Structures: a Physical Approach with Emphasis on Earthquake Engineering, Computers and Structures Inc., Berkeley, California, 2002.
[40] J. Wolf, Dynamic Soil Structure Interaction, Prentice-Hall, Englewood Cliffs, New Jersey, 1985.
[41] J. Lysmer, R. Kuhlemeyer, Finite dynamic model for infinite media, J. Eng. Mech. Div. 95 (4) (1969) 859–878.
[42] G. Sevieri, A. De Falco, M. Andreini, H.G. Matthies, Hierarchical Bayesian framework for uncertainty reduction in the seismic fragility analysis of concrete gravity dams, Eng. Struct. 246 (2021) 113001.
[43] G. Sevieri, A. De Falco, G. Marmo, Shedding light on the effect of uncertainties in the seismic fragility analysis of existing concrete dams, Infrastructures 5 (3) (2020) 22.
[44] G. Hatzigeorgiou, D. Beskos, D. Theodorakopoulos, M. Sfakianakis, A simple concrete damage model for dynamic FEM applications, Int. J. Comput. Eng. Sci. 2 (02) (2001) 267–286.
[45] O. Omidi, S. Valliappan, V. Lotfi, Seismic cracking of concrete gravity dams by plastic-damage model using different damping mechanisms, Finite Elem. Anal. Des. 63 (2013) 80–97.
[46] A. Chopra, Chapter 15: Earthquake response analysis of concrete dams, in: R. Jansen (Ed.), Advanced Dam Engineering for Design, Construction, and Rehabilitation, Van Nostrand Reinhold, New York, 1988.
[47] M.K. Poul, A. Zerva, Efficient time-domain deconvolution of seismic ground motions using the equivalent-linear method for soil-structure interaction analyses, Soil Dyn. Earthq. Eng. 112 (2018) 138–151.
[48] G.S. Sooch, A. Bagchi, A new iterative procedure for deconvolution of seismic ground motion in dam-reservoir-foundation systems, J. Appl. Math. (287605) (2014).
[49] A. Zerva, M. Falamarz-Sheikhabadi, P.M. K., Issues with the use of spatially variable seismic ground motions in engineering applications, in: Recent Advances in Earthquake Engineering in Europe, Chapter 9, Springer, ISBN: 978-3-319-75740-7, 2018, pp. 2269–2280.
[50] M.A. Hariri-Ardebili, V. Saouma, Single and multi-hazard capacity functions for concrete dams, Soil Dyn. Earthq. Eng. 101 (2017) 234–249.
[51] P. Giovenale, C. Cornell, L. Esteva, Comparing the adequacy of alternative ground motion intensity measures for the estimation of structural responses, Earthq. Eng. Struct. Dyn. 33 (2004) 951–979.
[52] P. Tothong, N. Luco, Probabilistic seismic demand analysis using advanced ground motion intensity measures, Earthq. Eng. Struct. Dyn. 36 (2007) 1837–1860.
[53] J. Padgett, B. Nielson, R. DesRoches, Selection of optimal intensity measures in probabilistic seismic demand models of highway bridge portfolios, Earthq. Eng. Struct. Dyn. 37 (2008) 711–725.
[54] M.A. Hariri-Ardebili, V. Saouma, Probabilistic seismic demand model and optimal intensity measure for concrete dams, Struct. Saf. 59 (2016) 67–85.
[55] USACE, Time-History Dynamic Analysis of Concrete Hydraulic Structures, Technical Report EM 1110-2-6051, Department of the Army, U.S. Army Corps of Engineers, Washington D.C., USA, 2003.
[56] B. Ellingwood, P. Tekie, Fragility analysis of concrete gravity dams, ASCE J. Infrastruct. Syst. 7 (2001) 41—48.
[57] H. Zhong, G. Lin, X. Li, J. Li, Seismic failure modeling of concrete dams considering heterogeneity of concrete, Soil Dyn. Earthq. Eng. 31 (12) (2011) 1678–1689.
[58] R. Chandramohan, J.W. Baker, G.G. Deierlein, Impact of hazard-consistent ground motion duration in structural collapse risk assessment, Earthq. Eng. Struct. Dyn. 45 (8) (2016) 1357–1379.
[59] M.A. Hariri-Ardebili, S. Sattar, Uncertainty and bias in fragility estimates by intensifying artificial accelerations, Probab. Eng. Mech. (2023) 103545.
[60] C. Cornell, H. Krawinkler, Progress and challenges in seismic performance assessment, 2000, http://peer.berkeley.edu/news/2000spring/index.html.
[61] J. Baker, C. Cornell, Uncertainty propagation in probabilistic seismic loss estimation, Struct. Saf. 30 (3) (2008) 236–252.

[62] M. Alembagheri, M. Seyedkazemi, Seismic performance sensitivity and uncertainty analysis of gravity dams, Earthq. Eng. Struct. Dyn. 44 (1) (2015) 41–58.
[63] A. Morales-Torres, I. Escuder-Bueno, L. Altarejos-Garcia, A. Serrano-Lombillo, Building fragility curves of sliding failure of concrete gravity dams integrating natural and epistemic uncertainties, Eng. Struct. 125 (2016) 227–235.
[64] G. Sevieri, M. Andreini, A. De Falco, H.G. Matthies, Concrete gravity dams model parameters updating using static measurements, Eng. Struct. 196 (2019) 109231.
[65] R.L. Segura, C. Bernier, C. Durand, P. Paultre, Modelling and characterizing a concrete gravity dam for fragility analysis, Infrastructures 4 (4) (2019) 62.
[66] M.A. Hariri-Ardebili, Uncertainty quantification of heterogeneous mass concrete in macro-scale, Soil Dyn. Earthq. Eng. 137 (2020) 106137.
[67] M.A. Hariri-Ardebili, C.L. Segura, S. Sattar, Modeling and material uncertainty quantification of RC structural components, Struct. Saf. 106 (2024).
[68] M. Dolšek, Estimation of seismic response parameters through extended incremental dynamic analysis, in: M. Papadrakakis, M. Fragiadakis, N.D. Lagaros (Eds.), Computational Methods in Earthquake Engineering, in: Computational Methods in Applied Sciences, vol. 21, Springer Netherlands, 2011, pp. 285–304.
[69] M. Alembagheri, M. Ghaemian, Seismic assessment of concrete gravity dams using capacity estimation and damage indexes, Earthq. Eng. Struct. Dyn. 42 (2013) 123–144.
[70] J. Baker, Efficient analytical fragility function fitting using dynamic structural analysis, Earthq. Spectra 31 (1) (2015) 579–599.
[71] M.A. Hariri-Ardebili, V. Saouma, Seismic fragility analysis of concrete dams: A state-of-the-art review, Eng. Struct. 128 (2016) 374–399.